Nanowire Superconducting Single Photon Detectors are Energy Detectors

J.J. Renema[1)], G. Frucci[2)], Z. Zhou[2)], F. Mattioli[3)], A. Gaggero[3)],
R. Leoni[3)], M.J.A. de Dood[1)], A. Fiore[2)], M.P. van Exter[1)]
1) Leiden Institute of Physics, Leiden University,
Niels Bohrweg 2, 2333 CA Leiden, the Netherlands
2) COBRA Research Institute, Eindhoven University of Technology,
P.O. Box 513, 5600 MB Eindhoven, The Netherlands and
3) Istituto di Fotonica e Nanotecnologie (IFN), CNR, via Cineto Romano 42, 00156 Roma, Italy

Using detector tomography, we demonstrate that the detection mechanism in NbN-based superconducting single photon detectors (SSPDs) is sensitive to the total energy. In addition, we demonstrate a scaling law for the interchange of bias current and excitation energy. These results are achieved by studying multiphoton excitations in a nanodetector with a sparsity-based tomographic method that allows factoring out of the optical absorption. We demonstrate this scaling law over the entire range of the experiment, from 0.9 eV to 3.8 eV. The tomographic method facilitates investigation of the fundamental physics of the detection events in NbN wires and demonstrates that nanodetectors provide a useful model system to understand more complicated wire geometries such as the meandering wire of a SSPD.

I. INTRODUCTION

Nanowire Superconducting Single Photon Detectors (SSPDs) [1] have high detection efficiency [2], low dark counts, low jitter and a broadband absorption spectrum [3]. This makes them suitable for many applications including quantum optics [4–7], quantum key distribution [8, 9], optical time domain reflectometry [10] and interplanetary communication [11]. These detectors typically consist of a thin nanowire (4 nm x 100 nm) of superconducting material, such as NbN [1], TaN [12], NbTiN [13], Nb [14], or WSi [2], which is typically fabricated in a meander shape to cover an active area of 25-1600 μm^2 [15]. The absorption of a single photon in the nanowire results in the creation of a a region with a non-equilibrium concentration of quasiparticles. When the nanowire is biased close to the critical current, this perturbation causes a transition from the superconducting to the resistive state, producing a voltage pulse in the external circuit.

It has long been known that at lower bias current, the detector operates in a regime where multiple photons are necessary to break the superconductivity [1, 16]. In meander-type SSPDs, this process is strongly surpressed, since if two photons are absorbed far apart along the wire, they do not constitute a single excitation and will not produce a detection event [17, 18].

In this publication, we use a NbN nanodetector to enhance these multiphoton excitations, with the aim of studying the physics of the detection process. We use a sparsity-based tomographic method, which can distinguish effects at different photon numbers, to study the various multiphoton effects in a single experiment [19]. This enhancement is achieved by using a nanodetector, which consists of a wire with a bowtie-shaped constriction geometry (see Fig 1) [20]. In this type of detector, the active area is defined by the geometric constriction, and all photons absorbed in this area participate in the detection process.

Our results consist of three parts.

i) We show that it is the overall energy of the excitation that determines the behaviour of the detector. An SSPD is therefore more properly thought of as an energy detector rather than a single-photon detector. We show that the response of the device is independent of the wavelength of the photons that constitute the excitation but only dependent on the total energy of the excitation. This quantitative comparison of different experimental settings is made possible by the use of a sparsity-based tomographic protocol. One further advantage of this method is that the coupling efficiency of the photons to the NbN film factors out.

ii) We demonstrate that over the range of our experiment, there is linear scaling behaviour between bias current and overall excitation energy. This scaling behaviour allows for an interchange between bias current and energy while keeping the detection probability constant. All three current microscopic models for detection events in SSPDs predict this linear behaviour to good approximation.

iii) We use this scaling law to rescale all our data. We demonstrate that after this rescaling, all of the response curves superimpose, creating a photoresponse curve as a function of the rescaled bias current that is universal over the energy range of the experiment. This demonstrates that the detection probability in our NbN nanodetector is only dependent on a specific combination of bias current and energy. This behaviour can only be identified because the tomographic method separates the contributions from different photon numbers and factors out the incoupling efficiency. This last result puts a constraint on any ab-initio theory describing the detection probability as a function of bias current and input energies: it must only depend on this given linear combination.

II. DETECTION EVENTS IN SSPDS

While big strides have been taken [21–24] in understanding the fundamental physics of these detectors, many details of the detection mechanism in such detectors are still unknown. After the absorption of a photon, it is thought that the resulting high-energy electron destroys Cooper pairs that carry the bias current, producing a cloud of quasi-particles [25, 26]. In some models, this breakdown is assisted by a thermal fluctuation process, such as a vortex crossing, which adds an extra perturbtion to the system. This process results in a breakdown of the superconductivity, resulting in a normal cross-section. After such a resistive barrier has formed, the kinetic inductance of the device drives Joule heating in the normal state area [27], causing it to grow. After that, the current drops to a negligible level [28] and the interplay between the cooling of the device and the restoration of the current determines whether the device returns to its previous state, ready to detect another photon.

Currently, there is no consensus on a microscopic model for the detection event in superconducting single photon detectors. Below, we briefly introduce three microscopic models for detection events in the SSPD from literature. We refer to these three as the normal-core hotspot model, the diffusion hotspot model and the fluctuation model. Each of these models predicts that the energy and current are exchangeable through a given scaling law, and their prediction will be compared with the experimental data below.

The *normal-core hotspot model* was introduced in the original papers reporting photodetection with SSPDs [1, 29]. In this model, it is assumed that the photon absorption creates a normal core inside the material. Current is then diverted around this core. If the current locally exceeds the critical current, superconductivity is destroyed and a normal state slab is created, resulting in a detection event. In this model, the current required to pinch off the entire channel for a given input energy goes as the square root of the energy, since the hotspot is assumed to be a cylindrical object inside the wire. For a given energy, the bias current I_b needed to achieve maximal detection efficiency is then given by:

$$E = \frac{w^2}{C^2}(1 - I_b/I_c)^2, \tag{1}$$

where E is the energy of the photon, I_b is the bias current and I_c is the critical current. w is the width of the wire and C is a scaling constant, which is defined in this way for consistency with previous work [30].

In the *diffusion-hotspot model*, which was introduced later as a refinement of the original normal-core hotspot model, the role of the diffusion of quasiparticles is taken into account, as well as the reduction of the critical current due to the quasiparticles [21, 25]. In this model, the relevant lengthscale is given by the diffusion length over a time characteristic for the cascade of quasiparticles. This expression, which was first derived in Ref. [25], predicts linear scaling between bias current and cutoff energy:

$$E = E_0(1 - I_b/I_c), \tag{2}$$

where E_0 is an energy scale [26].

Fluctuation model The previous two models predict a sharp cutoff of the detection efficiency as a function of photon energy, which is not observed in experiments. In order to explain the observed detection probability beyond the cutoff energy, fluctuation-assisted detection models have been proposed [22–25]. All of these have in common that the role of the photon in the detection process is to depress the superconducting gap. Subsequently, a thermally activated fluctuation occurs, such as the depairing of a vortex-antivortex pair (VAP) [31] in the superconductor or the crossing of a single vortex. This fluctuation must overcome an energy barrier $E(\Delta, I_b)$ [24]. Expressions for such energy barriers typically contain a gap-dependent energy scale and a current-dependent geometric factor [26]. The specifics of the geometric factor depends on the precise fluctuation process. Both for the VAP model and for the single-vortex crossing model, we can linearize the current-dependence of the geometric factor over the range of currents that was used in the experimernt. We obtain:

$$A = (\Delta - \alpha\sqrt{E})(I_0 - \beta I_b), \tag{3}$$

where the constants I_0 and β are known from the linearization of the geometric factor, and A and α are the experimental fit parameters. Such a model predicts a hyperbolic interchange between energy and current.

III. EXPERIMENT

All experiments in this work were performed on a nanodetector (see Fig 1). The nanodetector consists of 4 nm thin NbN wire on a GaAs substrate, shaped into a 150 nm wide bowtie geometry. The device was fabricated via a combination of DC magnetron sputtering [32], electron-beam litography, reactive ion etching and evaporation of the metal contacts [20]. In previous work [19, 20], it was shown that such a detector has multiphoton regimes based on the bias current. The physical mechanism behind these multiphoton regimes is that at relatively low bias currents, multiple photons are required to supply a sufficient perturbation for the superconductivity to be broken.

The device was cooled in a two-stage pulse-tube / Joule-Thompson cryocooler to a temperature of approximately 1.2K. The nanodetector was illuminated using a lensed fiber mounted on cryogenic nanomanipulators. At this temperature, the overall system detection efficiency for single photons was 1.5×10^{-4} around our working point at $I_b = 20\,\mu$A ($I_c = 29\,\mu$A) . This low efficiency is

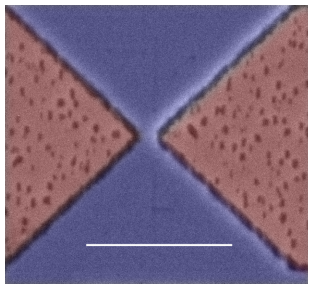

Figure 1: False-color SEM image of the detector. The active part of the detector is the narrow bridge in the centre of the image. The blue parts represent the thin layer of NbN, the red parts are the GaAs substrate. The scale bar has a length of 1 μm.

attributable to the mismatch between the device active area and the size of the illumination spot. The device was operated in a voltage bias regime, using a Yokogawa GS200 in series with a 10 Ω resistor. The detector was biased through the DC port of a bias tee, and the RF clicks were amplified in a 45 dB amplifier chain.

The device was illuminated with a Fianium Supercontinuum laser, whose pulse duration was specified to be 7 ps. It is crucial for this experiment that the pulse duration is shorter than the lifetime of an excitation, which is estimated to be several tens of picoseconds [33–35]; for longer pulse durations, it is possible to have a pulse which produces two excitations which are far enough apart in time as to not produce a single multiphoton excitation. The device was illuminated with narrowband light at wavelengths of 1000 nm, 1300 nm and 1500 nm ($\Delta\lambda$= 10 nm). In our experiment, we vary the intensity and wavelength of the input light, at various bias currents. At each of these settings, we record the count rates in a 0.1 s time window and repeat the experiment 10 times per measurement setting.

IV. TOMOGRAPHY OF MULTIPHOTON EXCITATIONS

In order to distinguish the effects of the various photon numbers in the laser pulses, we make use of a tomographic protocol. We illuminate the detector with a range of coherent states, and record the click probability R_{click}. Each illumination intensity probes the detector with a different linear combination of photon numbers, introducing different combinations of multiphoton excitations. Since we have many more experiments than photon numbers that are of interest, we obtain an overcomplete set of equations, which can be inverted using suitable techniques for such problems [36–38].

Since the physical size of the detector is much smaller than the wavelength, the incoupling must necessarily be very inefficient due to the diffraction-limited size of the illumination spot. To perform tomography in this geometry, we have established a sparse tomographic protocol.

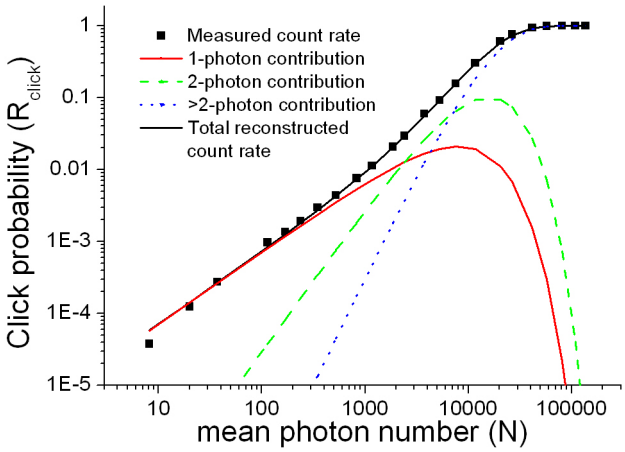

Figure 2: Illustration of the tomographic protocol. The black squares indicate the measured count rate as a function of input power, at λ = 1500 nm and I_b = 17 μA. The red and green lines show the contribution to the count rate of single photons and photon pairs, respectively. The blue line shows the contribution of higher numbers of photons. The black line shows the sum of all the photon contributions, indicating that our tomographic reconstruction succesfully reproduces the observed count rates. From this fit, we reconstruct the set of detection probabilities p_n and η which describes the behaviour of the detector.

This model was introduced in a previous publication [19], and we give here a brief summary of the main features. In this protocol, it is assumed that the number of parameters that describes the detector is small, and that most of the behaviour of the count rates is dominated by low incoupling efficiency. Using model selection rules [39], it is possible to find the description of the detector that requires the least number of parameters to be fully consistent with the experimental data , thus invoking the sparsity assumption. In particular, we model the click probability R_{click} by:

$$R_{click} = 1 - e^{-\eta N} \sum_{n=0}^{\infty} (1 - p_n) \frac{(\eta N)^n}{n!}, \qquad (4)$$

where η is the incoupling efficiency, and N is the mean photon number of the incident coherent state. The meaning of the set of p_n is as follows: the p_i are the parameters that describe all nonlinear (multiphoton) effects in the detector. They are therefore the quantity of interest in the further analysis of the behaviour of the detector. The linear efficiency η quantifies the linear effects in the detector, i.e. the probability that each individual photon participates in the detection process. In making this separation, we have used the fact that an attenuated coherent state is still a coherent state, with reduced mean photon number. This is reflected by the fact that in Eq. 4, only the combination ηN occurs.

We attribute the linear loss quantified by η to the combination of coupling of the beam to the detector area and absorption in the wires [19]. Each p_n indicates the probability that the detector clicks, given that n photons are absorbed in the active area and participate in the detection event. The probability of this occuring is assumed to be independent for each photon, and is given by the linear efficiency η. The separation between η and $\{p_n\}$ is therefore one between linear and nonlinear effects, respectively.

The infinite sum in Eq. 4 is truncated at some n_{max} by our model selection rule: we select the model with minimal reduced χ^2. This truncation enables us to recover both η and the set of nonlinear parameters p_n from a single experiment.

Fig. 2 illustrates this protocol as applied to a single experimental run for a given bias current. We vary the incident power, observe the click probability, and apply the procedure outlined in this section to find the contributions from the various multiphoton excitations. The black squares indicate the measured count probability, approaching 1 as the detector saturates. The red (solid), green (dashed) and blue (dotted) lines indicate the contribution from one photon, two photons and higher photon numbers, respectively. The remainder term, which contains the limit of high photon numbers, is not used in the results presented below. Fig. 2 shows that there is a low-power regime where the detector responds primarily to single-photon excitations, an intermediate regime where the detector responds to two-photon excitations, and a third regime where the detector is approaching saturation. The fact that the photon regimes split in this way with input power enables us to recover them seperately. Furthermore, since the linear efficiency η only rescales the effective incident photon number but does not alter its shape (corresponding to a simple shift in Fig 2), we are also able to distinguish finite incoupling effects from effects due to multiphoton excitations.

V. RESULTS

Figures. 3-5 present our main results. Fig 3 shows the reconstructed detection probabilities p_n, as a function of bias current and for different wavelengths. For each wavelength and current, we independently perform the tomographic procedure outlined in section IV and obtain a full set of nonlinear parameters p_n.We observe that as the current is lowered, the detector makes a transition from being a one-photon detector to a two-photon detector, and so on. Furthermore, we observe that the response curves at different photon numbers and wavelengths have the same shape. We note that as the excitation energy becomes higher and the photon number larger, the points on our curves become more scattered, indicating that the tomography procedure becomes less accurate.

Fig. 4 demonstrates that there is a scaling law be-

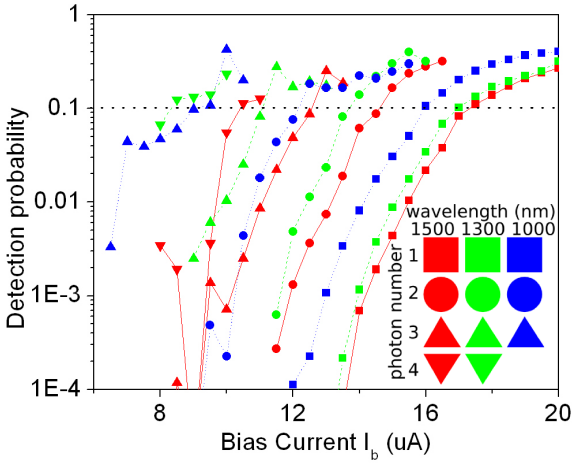

Figure 3: Current dependence of the nonlinear parameters p_n , as a function of wavelength and photon number. The probability p_n of the detector clicking at a given wavelength and photon number is plotted as a function of the current. The plots are color-coded by wavelength. The shape of the symbols indicates the photon number (see legend). The connecting lines are a guide to the eye. The dotted line indicates the threshold level used to obtain Fig. 4.

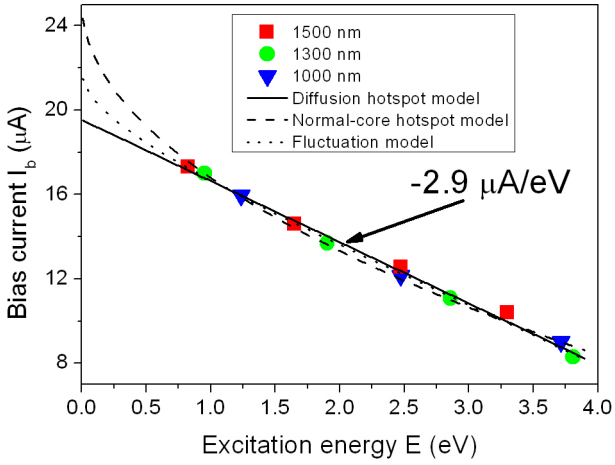

Figure 4: Scaling law for the nanodectector. From the data in Fig 3, we find all points that have $p_n(E, I_b) = 0.1$ (indicated by the dotted line in that figure), where E is the overall excitation energy. In this graph, we plot the values of I_b and E that satisfy this condition. This graph shows that bias current and overall excitation energy have a linear dependence. Furthermore, the fact that points at various photon numbers all fall on the same line demonstrates that the nanodetector is only sensitive to the overall energy of the excitation. The three lines show the fits of the three microscopic models to the data.

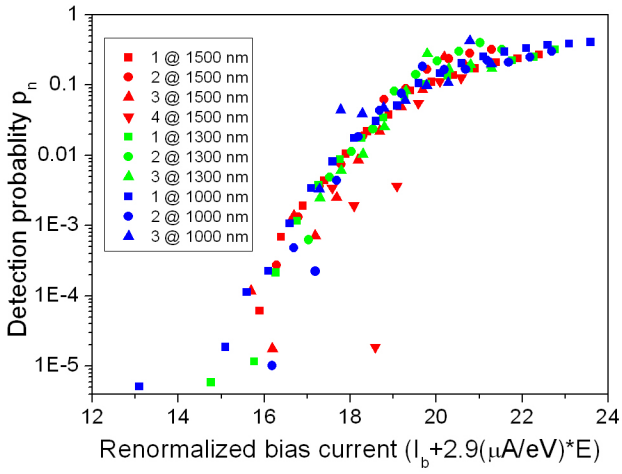

Figure 5: Universal response curve for the nanodetector. To obtain these curves, we rescale the curves reported in Fig. 3 by the scaling law demonstrated in Fig. 4.

tween bias current and overall excitation energy. In order to obtain this figure, we took a surface of constant $p_n(E, I_b) = 0.1$ in Fig. 3 (indicated by a dotted line), and plotted the bias current at which the detector has 10% probability of responding to an energy E, where $E = nh\nu$ is the total energy of the n photons absorbed by the detector. The three curves in Fig. 4 show the best fit of the three microscopic models to the data. Over the range of the experiment, the predictions for the three models are to good approximation equivalent: they all predict the observed linear interchange between photon energy and bias current. Only below E $<$ 0.5 eV do the three models differ significantly. Fig. 4 shows that there is a scaling law between current and energy: in our detector, they are interchangebale at a rate γ of γ = -2.9 $\pm$ 0.1 μA/eV (= -1.8×10^{13} Wb^{-1}in SI units).

In Fig 5, we apply the scaling law and find that all the curves of detection probability as a function of rescaled bias current superimpose over 5 orders of magnitude in the detection probability. This shows that the photoresponse of our detector depends only on this specific combination of bias current and excitation energy. We stress that this universal curve can only be obtained through detector tomography that allows separation of the effects of multiphoton excitation and finite linear efficiency.

Since the curve is universal over 5 orders of magnitude in the detection probability, we have demonstrated that our results are independent of the arbitrary choice of the 10% criterion. The criterion only matters for the accuracy with which the curves can be superimposed: we find from theoretical simulations that the tomographic reconstruction is most accurate between $p_n = 0.1$ and $p_n = 10^{-5}$. This justifies the choice of our criterion.

VI. DISCUSSION

In this section, we first compare our experimental method with that of previous studies on SSPDs. Then, we discuss our three experimental findings: energy detection, linear interchange between bias and energy and the universal detection curve. Lastly, we discuss the phenomenon of dark counts in our detector.

Comparison with previous work Our present method has three advantages over methods used in previous studies, in which SSPDs were studied by varying the wavelength of the incident light [25, 26]. First of all, through a tomographic method, we obtain a full quantitative description of our detector. This description allows comparison of different detection settings, enabling us to find the scaling law reported in Section IV. Secondly, our tomographic protocol can distinguish various multiphoton excitations, which enables us to extend the results from previous work to the multiphoton regime. Thirdly, since the linear absorptance is factored out by the fitting procedure, the derived detector response parameters p_n are independent of the coupling efficiency and absorptance. In particular, the wavelength dependence of the optics inside the cryostat, of the absorption into the NbN and of any associated cavity structure [40] is removed. This strongly facilitates quantitative comparison between different experimental settings.

Multiphoton excitation has the very practical advantage that the bandwidth of energy excitations which is offered can be extended by a factor equal to the number of photons in the highest excitation (in our case, 4). This has applications in the situation where light of a particular wavelength is difficult to couple onto a cryogenic sample. In this way, we extend the available energy range of excitations for any given cryogenic setup. In particular, the present work opens up the possibility of studying NbN detector behaviour in an energy range which corresponds to the near and medium UV range.

The tomographic method does not require a model of the device, which makes it useful as a tool for investigating the working principle of any type of detector. SSPDs are an important case study for the application of the tomographic method, since they possess both nontrivial detection statistics [17, 18], and their working mechanism is not fully understood yet.

Energy detection. The fact that only the overall energy of the excitation determines the response of the photodetector can be interpreted in terms of the cascade process that generates the initial excitation. This process, which is thought to involve both electrons and phonons in the film, and in which the mutual exchange of energy between the electron and phonon subsystem plays a key role, is still poorly understood. In the present work, we probe this cascade process with different initial excitations, and show that it is only the overall energy which determines the total number of quasiparticles which are produced at the superconducting band-edge. The fact that four excitations of a quarter of the energy produce the same

number of QP as a single excitation with the full energy is evidence of the fact that the conversion efficiency by which the energy of the first QP is distributed over many others is independent of the initial energy.

In the normal-core hotspot model, multiphoton events can only occur if the various normal cores are created at the cross-section of the wire. Given the relative size of our detector and the size of the normal cores in this hotspot model, we would expect to see reduced count rates at high photon numbers due to the low probability of several photons being absorbed at exactly the same point in our detector. The fact that we do not observe such reduced count rates is evidence the in our experiment, the size of the hotspot is comparable to the size of our detector.

Linear interchange We apply the three models, and compare the results with the values from literature. For the normal-core hotspot model, we find $C = 46$ $\mathrm{eV}^{-1/2}/$ nm, which should be compared to the values of $C = 11 - 20$ $\mathrm{eV}^{-1/2}/$ nm found in other experiments [3]. For the diffusion hotspot model, we apply the expression from Ref. [26], to find a theoretical value of γ = -2.5 μA/eV for our sample and γ = -3.5 μA/eV for the samples in that reference, which should be compared with the value of γ = -2.9 μA/eV obtained experimentally. We note, however, that this result depends linearly on the assumed conversion efficiency ς of the initial excitation into quasiparticles, which varies strongly from detector to detector. For the fluctuation model, we find $\alpha = 2.2 \times 10^{-4}\sqrt{\mathrm{eV}}$, which should be compared to a literature value of $\alpha = 6 \times 10^{-4}\sqrt{\mathrm{eV}}$, for the experiment reported in Ref. [31].

We note that in all three models, there is one overall scale parameter which is meaningless, because its value depends on the precise choice of the threshold criterion in Fig 3. In the two hotspot models, this introduces an offset current. In the fluctuation model, the energy scaling constant A depends on the choice of the threshold criterion.

Universal detection curve By demonstrating a universal detection curve, we have shown that the various models for photodetection do not just predict the scaling behaviour for the plateau region of the detection efficiency, but for the entire detection curve. Such quantitative comparison would not be possible without the use of the tomographic method.

In a previous publication [35], we have introduced the notion of the nonlinear response function (NRF) $\eta(I_b, C)$, which measures the instantaneous click probability, given that a bias current of I_b is present, and that there are C quasiparticles in the detector. The overall click probability is then given by $\mathrm{R} = \int_t \eta(t) I(t) dt$, where I is the instantaneous intensity. This function may be probed through various means, such as measuring the autocorrelation in a pump-probe experiment. The description in terms of a NRF is well-matched to a tomographic experiment, as both are model-independent descriptions.

The holy grail of tomographic research on SSPDs would be to find the instantaneous click probability as a function of the number of quasiparticles present at that instant. In the present experiment, we have achieved a step towards this goal: we have demonstrated the NRF to be of the form $\eta(I_b + \gamma E)$ over the energy range of the experiment.

Dark counts We now turn to the phenomenon of dark counts. Extrapolating the linear scaling law from Fig. 4 to $E = 0$ yields a current of 19 μA. However, the actual dark count rate at this current was negligibly small; we only observe appreciable dark counts around the critical current of 29 μA. The same issue holds for the extrapolations from the other two models. Therefore, our scaling law does not hold for dark counts. For this, we propose the following explanation: due to the geometry of our detector, there will always be a vortex pair present at the corners of the detector. When a photon is absorbed, the vortex pair is depinned, and the energy contained in it is added to the excitation. However, when there is no photon present, the vortex pair must tunnel through an energy barrier, producing a much lower dark count rate. The energy barrier for a single vortex to cross our detector is of the order of 20 meV in our sample [26].

The anomalous behaviour of dark counts is a reminder of the danger of assuming a detection model, further demonstrating the relevance of our tomographic method. In particular in this case, the tomographic method may give the first hints of substantial differences in detection mechanism between dark counts and light counts. While we have proposed an explanation for this behaviour in terms of vortex pairs which is consistent with the data, we note that the nature of dark counts is still open to debate [22–24].

VII. CONCLUSIONS

We have studied the physics of photodetection in a superconducting single photon detector. We have shown three main results. First, we have shown that the detection is based on the overall energy of the excitation. Second, that there is a scaling law between overall excitation energy and bias current. Third, that there is a universal response curve that depends only on a given combination of bias current and excitation energy. Thereby, we have shown that the known behaviour of the detector extends into the multiphoton range. These results demonstrate that the tomographic method is a useful tool for investigating the fundamenal physics of detection events in NbN SSPDs. Our technique extends the available range of energy excitations beyond that of a given cryogenic setup, and we have shown that the nanodetector is a useful model of a single cross-section of a meander-type SSPD.

Acknowledgments

We thank D. Sahin for providing the SEM image of the detector. We thank Prof. G. Goltsman, Prof. P. Kes, Prof. J Aarts, Q. Wang and R. J. Rengelink for useful discussions. This work is part of the research programme 'Nanoscale Quantum Optics' of the Foundation for Fundamental Research on Matter (FOM), which is financially supported by the Netherlands Organisation for Scientific Research (NWO) and is also supported by NanoNextNL, a micro- and nanotechnology program of the Dutch Ministry of Economic Affairs, Agriculture and Innovation (EL&I) and 130 partners, and by the European Commission through FP7 project Q-ESSENCE (contract No. 248095).

[1] G. N. Goltsman, O. Okunev, G. Chulkova, A. Lipatov, A. Semenov, K. Smirnov, B. Voronov, A. Dzardanov, C. Williams, and R. Sobolewski, Appl. Phys. Lett. **79**, 705 (2001), ISSN 00036951.

[2] F. Marsili, V. B. Verma, J. A. Stern, S. Harrington, A. E. Lita, T. Gerrits, I. Vayshenker, and B. Baek (2012), arXiv:1209.5774.

[3] A. Verevkin, J. Zhang, R. Sobolewski, A. Lipatov, O. Okunev, G. Chulkova, A. Korneev, K. Smirnov, G. N. Gol'tsman, and A. Semenov, Appl. Phys. Lett. **80**, 4687 (2002), ISSN 00036951.

[4] M. J. Stevens, B. Baek, E. A. Dauler, A. J. Kerman, R. J. Molnar, S. A. Hamilton, K. K. Berggren, R. P. Mirin, and S. W. Nam, Opt. Express **18**, 1430 (2010), ISSN 1094-4087.

[5] C. Zinoni, B. Alloing, L. H. Li, F. Marsili, A. Fiore, L. Lunghi, A. Gerardino, Y. B. Vakhtomin, K. V. Smirnov, and G. N. Goltsman, Appl. Phys. Lett. **91**, 031106 (2007), ISSN 00036951.

[6] M. Halder, A. Beveratos, M. Gisin, V. Scarani, C. Simon, and H. Zbinden, Nat. Phys. **3**, 692 (2007).

[7] J. Renema, G. Frucci, M. de Dood, R. Gill, A. Fiore, and M. van Exter, Phys. Rev. A **86**, 062113 (2012).

[8] R. H. Hadfield, J. L. Habif, J. Schlafer, R. E. Schwall, and S. W. Nam, Appl. Phys. Lett. **89**, 241129 (2006), ISSN 00036951.

[9] R. Collins, R. Hadfield, V. Fernandez, S. Nam, and G. Buller, Electron. Lett. **43**, 180 (2007), ISSN 00135194.

[10] N. Mohan, O. Minaeva, G. N. Goltsman, M. B. Nasr, B. E. Saleh, A. V. Sergienko, and M. C. Teich, Opt. Express **16**, 18118 (2008), ISSN 1094-4087.

[11] D. M. Boroson, J. J. Scozzafava, D. V. Murphy, and B. S. Robinson, 2009 Third IEEE International Conference on Space Mission Challenges for Information Technology pp. 23–28 (2009).

[12] A. Engel, A. Aeschbacher, K. Inderbitzin, A. Schilling, K. Il'in, M. Hofherr, M. Siegel, A. Semenov, and H.-W. Hübers, Appl. Phys. Lett. **100**, 062601 (2012), ISSN 00036951.

[13] S. N. Dorenbos, E. M. Reiger, U. Perinetti, V. Zwiller, T. Zijlstra, and T. M. Klapwijk, Appl. Phys. Lett. **93**, 131101 (2008), ISSN 00036951.

[14] A. Annunziata, D. Santavicca, J. Chudow, L. Frunzio, M. Rooks, A. Frydman, and D. Prober, IEEE Transactions on Applied Superconductivity **19**, 327 (2009), ISSN 1051-8223.

[15] F. Mattioli, M. Ejrnaes, A. Gaggero, A. Casaburi, R. Cristiano, S. Pagano, and R. Leoni, J. Vac. Sci. Technol. **30** (2012).

[16] J. Zhang, W. Slysz, A. Pearlman, A. Verevkin, R. Sobolewski, O. Okunev, G. Chulkova, and G. Goltsman, Phys. Rev. B **67**, 132508 (2003), ISSN 0163-1829.

[17] M. K. Akhlaghi, A. H. Majedi, and J. S. Lundeen, Opt. Express **19**, 21305 (2011).

[18] M. K. Akhlaghi and A. H. Majedi, IEEE Trans. Appl. Supercond. **19**, 361 (2009).

[19] J. J. Renema, G. Frucci, Z. Zhou, F. Mattioli, A. Gaggero, R. Leoni, M. J. A. D. Dood, A. Fiore, and M. P. V. Exter, Opt. Express **20**, 2806 (2012).

[20] D. Bitauld, F. Marsili, A. Gaggero, F. Mattioli, R. Leoni, S. Jahanmirinejad, F. Lévy, and A. Fiore, Nano Lett. **10**, 2977 (2010), ISSN 1530-6992.

[21] A. Engel, K. Inderbitzin, A. Schilling, R. Lusche, A. Semenov, D. Henrich, M. Hofherr, K. Il, and M. Siegel (2012), arXiv:1210.5395v1.

[22] A. Gurevich and V. Vinokur, Phys. Rev. B **86**, 026501 (2012), ISSN 1098-0121.

[23] A. Gurevich and V. Vinokur., Phys. Rev. Lett. **100**, 227007 (2008), ISSN 0031-9007.

[24] L. Bulaevskii, M. Graf, C. Batista, and V. Kogan, Phys. Rev. B **83**, 144526 (2011), ISSN 1098-0121.

[25] A. Semenov, A. Engel, H.-W. Hübers, K. Il'in, and M. Siegel, Euro. Phys. J. B **47**, 495 (2005), ISSN 1434-6028.

[26] M. Hofherr, D. Rall, K. Ilin, M. Siegel, A. Semenov, H.-W. Hübers, and N. A. Gippius, J. Appl. Phys. **108**, 014507 (2010), ISSN 00218979.

[27] A. J. Kerman, E. A. Dauler, W. E. Keicher, J. K. W. Yang, K. K. Berggren, G. Goltsman, and B. Voronov, Appl. Phys. Lett. **88**, 111116 (2006), ISSN 00036951.

[28] A. J. Kerman, E. A. Dauler, J. K. W. Yang, K. M. Rosfjord, V. Anant, K. K. Berggren, G. N. Goltsman, and B. M. Voronov, Appl. Phys. Lett. **90**, 101110 (2007), ISSN 00036951.

[29] A. D. Semenov and A. A. Korneev, Physica C **351**, 349 (2001).

[30] K. Suzuki, S. Shiki, M. Ukibe, M. Koike, S. Miki, Z. Wang, and M. Ohkubo, Applied Physics Express **4**, 083101 (2011), ISSN 1882-0778.

[31] A. D. Semenov, P. Haas, H.-W. Hübers, K. Ilin, M. Siegel, A. Kirste, T. Schurig, and A. Engel, Physica C **468**, 627 (2008), ISSN 09214534.

[32] A. Gaggero, S. Jahanmirinejad, F. Marsili, F. Mattioli, R. Leoni, D. Bitauld, D. Sahin, G. J. Hamhuis, R. Nötzel, R. Sanjines, et al., Appl. Phys. Lett. **97**, 151108 (2010), ISSN 00036951.

[33] K. Ilin, M. Lindgren, M. Currie, A. Semenov, G. Goltsman, R. Sobolevski, S. Cherednichenko, and E. Gershenzon, Appl. Phys. Lett. **76**, 2752 (2000).

[34] D. Rall, P. Probst, M. Hofherr, S. Wünsch, K. Il'in, U. Lemmer, and M. Siegel, Journal of Physics: Confer-

ence Series **234**, 042029 (2010), ISSN 1742-6596.

[35] Z. Zhou, G. Frucci, F. Mattioli, A. Gaggero, S. Jahanmirinejad, T. B. Hoang, and A. Fiore (2012), arXiv:1209.2747v1.

[36] J. S. Lundeen, A. Feito, H. Coldenstrodt-Ronge, K. L. Pregnell, C. Silberhorn, T. C. Ralph, J. Eisert, M. B. Plenio, and I. A. Walmsley, Nat. Phys. **5**, 27 (2008), ISSN 1745-2473.

[37] A. Feito, J. S. Lundeen, H. Coldenstrodt-Ronge, J. Eisert, M. B. Plenio, and I. A. Walmsley, New J. Phys. **11**, 093038 (2009), ISSN 1367-2630.

[38] C. Natarajan, L. Zhang, H. Coldenstrodt-Ronge, G. Donati, S. Dorenbos, V. Zwiller, I. Walmsley, and R. Hadfield, Opt. Express **21**, 893 (2013).

[39] K. Burnham and D. Anderson, *Model selection and multimodel inference* (Springer, 1998).

[40] K. M. Rosfjord, J. K. W. Yang, E. A. Dauler, A. J. Kerman, V. Anant, B. M. Voronov, G. N. Goltsman, and K. K. Berggren, Opt. Express **14**, 527 (2006), ISSN 1094-4087.